Design Analysis of a High-Resolution Panoramic Camera Using Conventional Imagers and a Mirror Pyramid

Hong Hua, *Member*, *IEEE*,
Narendra Ahuja, *Fellow*, *IEEE*, and
Chunyu Gao, *Student Member*, *IEEE*

Abstract—Wide field of view (FOV) and high-resolution image acquisition is highly desirable in many vision-based applications. Several systems have reported the use of reflections off mirror pyramids to capture high-resolution, single-viewpoint, and wide-FOV images. Using a dual mirror pyramid (DMP) panoramic camera as an example, in this paper, we examine how the pyramid geometry, and the selection and placement of imager clusters can be optimized to maximize the overall panoramic FOV, sensor utilization efficiency, and image uniformity. The analysis can be generalized and applied to other pyramid-based designs.

Index Terms—Panoramic camera, mirror pyramids, omnidirectional imaging, and catadioptric systems.

1 Introduction

High-resolution, wide field of view (FOV), video rate image capture is highly desirable in many applications such as teleconferencing, surveillance, and robot navigation [21]. Imaging from a single viewpoint with a large depth-of-field is also preferred in some applications such as 3D reconstruction and rendering [1], [11], [19]. However, the FOV, resolution, and depth of field of a conventional digital camera are limited by the choice of imaging sensors and optics.

Many approaches have been presented to achieve various subsets of the desirable properties listed above, which fall into one of the two categories: dioptric and catadioptric methods [2]. Most of them use one or multiple regular cameras, which are hereafter referred to as imagers. Typical dioptric cameras include the imager cluster method [15], the fisheye method [18], and the rotating camera method [9], [16]. The catadioptric cameras include the designs capturing scenes through a single curved mirror with a single imager [1], [3], [5], [7], [14], [19], [21] and designs acquiring scenes reflected off planar mirror faces with multiple imagers [4], [6], [8], [10], [11], [12], [13], [17].

Among the numerous approaches, several systems use reflections off planar mirrors, which are usually assembled in the shape of mirror pyramids (MP) or prisms, to acquire high-resolution images from single or multiple viewpoints. Each imager, capturing part of the scene reflected off one of the flat mirror faces, is placed such that the mirror images of all imagers are colocated at a common viewpoint. Images from these imagers are then concatenated to yield a wide-FOV panoramic image. Nalwa first reported an implementation using a 4-sided single mirror pyramid (SMP) and four imagers [11]. A few alternative designs were proposed to achieve single-viewpoint or multiple-viewpoint panoramic imaging using a mirror-pyramid and its kin [4], [6], [8], [10], [12], [13], [17]. For instance, Hua and Ahuja presented a panoramic design using a dual mirror-pyramid (DMP) with two layers of imager clusters to double the vertical FOV of a panorama while preserving the ability to acquire high-resolution images from an apparent single viewpoint [6]. A similar design was proposed by Majumder et al. to create smooth mosaic of panoramas by image warping transformations after rough geometrical alignment [10]. Gao et al. described a design to acquire hemispherical panoramic images using a hexagonal prism [4].

In order to maximize the overall FOV, sensor usage, and image uniformity of a MP-based panoramic camera, it is critical to optimize the geometry of a pyramid shape, the placement of imagers, and the selection of imager parameters. In this paper, using a DMP-based camera as an example, we

1. define the geometrical and optical parameters that characterize a DMP-based camera (Section 2),
2. analyze the geometrical constraints for maximal panoramic FOV, which guide an optimal placement of imagers and the design of pyramid geometry (Section 3),
3. analyze the optical constraints for optimal sensor utilization and image uniformity, which guide the selection of the imager parameters (Section 4), and
4. demonstrate the application of the above analyses in a DMP camera prototype (Section 5).

2 Characterization of DMP-Based Panoramic Camera

A DMP panoramic camera consists of a dual-mirror pyramid (DMP) and two layers of imager clusters for single-viewpoint imaging or more clusters for multiviewpoint imaging [6], [17]. Each layer of the imager clusters is associated with one of the pyramids and each imager captures the scene reflected off its associated mirror face. The imagers in the clusters are positioned such that they share a common virtual viewpoint. With two layers of imagers per viewpoint, the FOV of an individual imager gets extended horizontally, by the two imagers associated with adjacent faces in the same pyramid, and vertically, by the imager associated with the adjacent face in the other pyramid. In the following sections, we define the parameters (Table 1) that characterize the DMP, imager clusters, and the camera systems, respectively.

2.1 Dual Mirror Pyramid

A DMP is formed by stacking back to back two N-sided right mirror-pyramids, $A_1A_2 \dots A_N - B_1B_2 \dots B_N$ and $D_1D_2 \dots D_N - B_1B_2 \dots B_N$ (referred to as pyramid A and D, respectively), such that their bases coincide (Fig. 1a). It can be characterized by the number of mirror faces, N, of a single pyramid, the slope angle formed by a mirror face with the pyramid base, and the base and cap radii which refer to the radii of the inscribed circles of the base or cap polygons. The two pyramids are assumed to have the same slope angle, α, and have a unit base radius and cap radii of r_a and r_d for the pyramids A and D, respectively. For nonunit DMPs, r_a and r_d are the ratios of the actual cap radii to the base radius.

Two other parameters of a pyramid shape, span angle and shape factor, are derived from the basic properties (Fig. 1a). The span angle, γ, refers to the angle subtended by the base edge of each face at the center of its base polygon, and is given as $\gamma = 360^\circ/N$. The shape factor is defined as the ratio of the height of a truncated pyramid to its base radius. The shape factors of the pyramids A and D are given by $s_a = (1 - r_a)\tan\alpha$ and $s_d = (1 - r_d)\tan\alpha$, respectively.

2.2 Imager Clusters

The usage of identical imagers is assumed. The intrinsic parameters of an imager include the focal length, f (mm), of the lens, the horizontal and vertical extents, $p(mm)$ and $q(mm)$, of the sensor, the number of horizontal and vertical pixels, $S(pixels)$ and

- *H. Hua is with the College of Optical Sciences, The University of Arizona, 1630 E University Blvd., Tucson, AZ 85721. E-mail: hhua@optics.arizona.edu.*
- *N. Ahuja and C. Gao are with the Beckman Institute, University of Illinois at Urbana-Champaign, 450 N Mathews Ave., Urbana, IL 61801. E-mail: {ahuja, cgao}@vision.ai.uiuc.edu.*

Manuscript received 22 Oct. 2005; revised 6 Feb. 2006; accepted 12 June 2006; published online 13 Dec. 2006.
Recommended for acceptance by K. Daniilidis.
For information on obtaining reprints of this article, please send e-mail to: tpami@computer.org, and reference IEEECS Log Number TPAMI-0563-1005.

TABLE 1
The Geometrical and Optical Parameters of a DMP-Based Camera

Dual Mirror Pyramid		Imager Cluster		DMP Camera System	
Number of mirror faces	N	Focal length(mm)	f	FOV	$360^\circ \times \theta_v$
Slope angle (degree)	α	Sensor size(mm)	$p \times q$	Sensor efficiency	e
Base radius	1	Sensor resolution (pixels)	$S \times T$	Effective resolution	$S \times T \times e$
Cap radii of pyramid A & D	r_a, r_d	Sensor center offsets (pixels)	$u_0 \times v_0$	Non-uniformity	U
Span angle (degree)	γ	Image-pyramid size ratio	r_c	Radial distortions	
Shape factors of pyramid A & D	s_a, s_d	Viewpoint offset (mm)	h	Keystone distortion	
		Imager orientation (degrees)	θ_T		

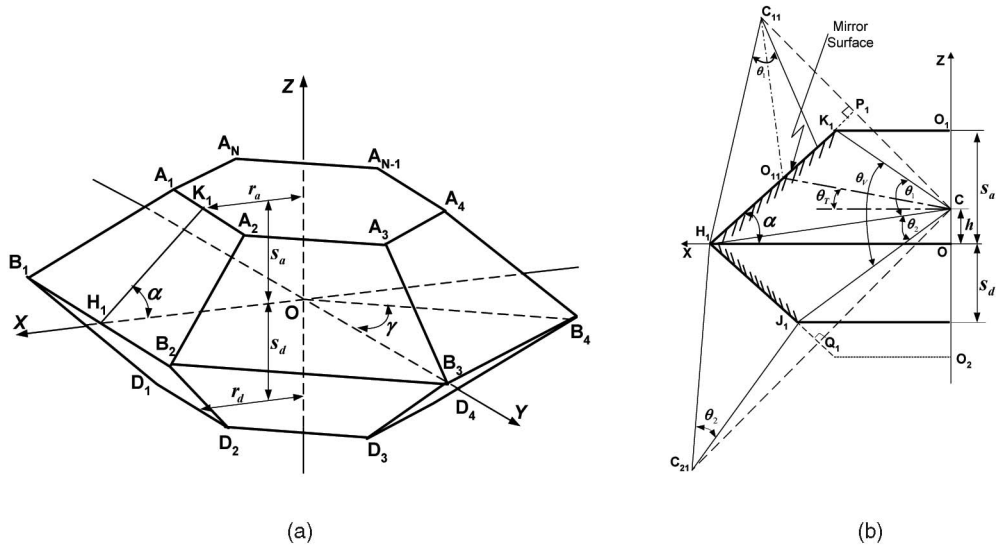

(a) (b)

Fig. 1. A DMP panoramic camera: (a) DMP geometry. (b) The placement of imager clusters and panoramic field of view.

$T(pixels)$, of the sensor, and the horizontal and vertical offsets, $u_0(pixels)$ and $v_0(pixels)$, of the sensor center from the intersection of the optical axis with sensor plane [20]. The physical dimensions of an imager are related to the visual angle of the self-occlusion region. The size of an imager is characterized with the radius of a sphere that encloses the imager body, and the ratio, r_c of the sphere radius to the radius of the pyramid base, is referred to as the imager-pyramid size ratio (Fig. 2).

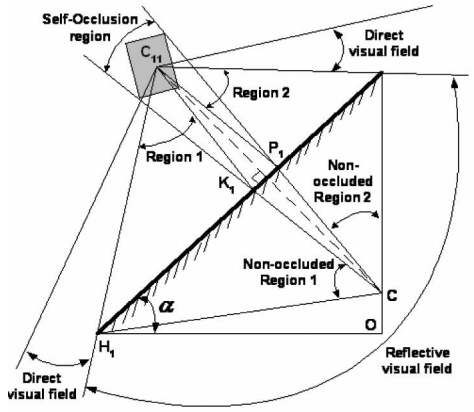

Fig. 2. Illustration of visual fields captured by a single imager through a pyramid face.

All the imagers per viewpoint are positioned such that their mirror images coincide at a common virtual viewpoint inside the pyramid. We define a 3D coordinate system $OXYZ$, in which the origin O coincides with the center of the pyramid base, the XY plane is parallel to the pyramid base OB_1B_2, the X-axis is normal to the base edge B_1B_2, and the Z-axis is perpendicular to the base (Fig. 1a). The common virtual viewpoint, C, is located on the symmetrical axis of the pyramid. The position of each imager is uniquely defined by the vertical offset, h, of the point C from the pyramid base.

The orientation of an imager is defined by the tilt angle between the mirror image (e.g., CO_{11}) of its physical optical axis (e.g., $C_{11}O_{11}$) and the pyramid base. Though it can have up to three degrees of freedom relative to its associated mirror face, its azimuth angle relative to the OXZ plane and the twist angle for the rotation around the optical axis are set to be zero. The tilt angle relative to the base plane, θ_T, of each imager is usually selected to maximize the sensor utilization (Fig. 1b).

2.3 DMP-Based Panoramic Camera

Assuming that each imager has a sufficiently large FOV, the scene captured through a mirror consists of two components: a scene reflected off the pyramid faces, referred to as reflective visual field, and a scene directly reaching the imager, referred to as direct visual field (Fig. 2). While the reflective visual field usually represents a contiguous panoramic view, if not properly designed, it may be subjected to self-occlusion by the physical imagers, and can be divided into three regions: the bottom nonoccluded region 1, the top

nonoccluded region 2, and the in-between self-occlusion region (Fig. 2). Practically, the self-occlusion region always creates a gap between regions 1 and 2. In a DMP-based camera, only the bottom region, close to the pyramid base, is optimized for panoramic capturing to ensure scene contiguity in the vertical direction. The FOV of a DMP-based panorama is the angular range of a contiguous scene that is reflected off the pyramid faces, free from occlusion caused by the physical imagers or any other fixture. If both the pyramid and imagers are designed appropriately, the reflected visual fields captured by the imagers can be seamlessly mosaiced. Therefore, the horizontal FOV of a DMP-based panorama is 360 degrees, and the vertical FOV, θ_V, is given as $\theta_V = \theta_1 + \theta_2$. θ_1 and θ_2 are the vertical nonoccluded FOVs by a vertical pair of mirror faces, respectively (Fig. 1b). They depend on the FOV of each imager, the pyramid geometry, and imager placement.

Besides FOV, the quality of a panorama can be further characterized by the measurements of its pixel resolution, sensor utilization, image uniformity, and radial distortion. Due to the tilt of the virtual optical axes of the imagers to the pyramid base, the reflective visual field is subject to the well-known keystone distortion effect. These properties will be defined in Section 4.

3 Geometrical Constraints for Optimizing Panoramic FOV

In order to maximize the overall panoramic FOV of the camera, we analyze the geometrical constraints and conditions that guide the optimal placement of imager clusters (Section 3.1), and optimize the design of pyramid geometry (Section 3.2).

3.1 Optimal Viewpoint Placement

The placement of the virtual viewpoint, along the pyramid axis, can vary from positions below the pyramid base to placements above the base (Fig. 1b). However, the viewpoint offset, h, is required to be 1) no more than the height of a single pyramid, $H = \tan\alpha$, 2) no more than $H_0 = \tan\alpha - \frac{r_c}{2\sin\alpha\cos\alpha\sin(\gamma/2)}$ to accommodate N imagers with sufficient space, and 3) no more than the critical value, $H_C = 1/\tan\alpha$, where one of the nonoccluded reflective visual fields due to the pyramids A and D varnishes (Fig. 2). With these requirements, the viewpoint offset is then constrained by

$$-H_{\max} \le h \le H_{\max}, \tag{1}$$

where $H_{\max} = \min(H, H_0, H_C)$. Applying this constraint of viewpoint placement, we can obtain the nonoccluded vertical FOVs by a vertical pair of mirror faces (Fig. 1b) and their sum gives the overall vertical FOV of a DMP camera, θ_V, as

$$\theta_V = 180 - 2\alpha - \theta_G, \tag{2}$$

where θ_G is the overall self-occlusion gap by an imager pair and is given by

$$\begin{aligned}\theta_G &= \frac{\theta_{G1} + \theta_{G2}}{2} \\ &= \tan^{-1}\left(\frac{r_c}{2(\sin\alpha - h\cos\alpha)}\right) + \tan^{-1}\left(\frac{r_c}{2(\sin\alpha + h\cos\alpha)}\right).\end{aligned} \tag{3}$$

The occlusion gap can be controlled within 5 degrees for the imager-pyramid size ratio of 5 percent, and within 10 degrees for the size ratio of 10 percent.

Equations (2) and (3) indicate that the overall vertical FOV and self-occlusion gap are independent of the number of mirror faces in a pyramid. It is easy to prove that placing the common viewpoint at the pyramid center in a DMP design (i.e., $h = 0$) minimizes the occlusion gap and maximizes the overall vertical FOV. In a single-view DMP camera, we designate the pyramid center as the common viewpoint. All mirror face-imager pairs are symmetrical and we use the parameters of the mirror face, $A_1A_2B_1B_2$, and its associated imager, C_{11}, to characterize the panoramic imaging system. The virtual optical axis of the imager, CO_{11}, collapses to OO_{11}.

3.2 Optimal Pyramid Geometry

Equations (2) and (3) further indicate that a small slope angle and a small imager-pyramid size ratio are preferred to achieve a large nonoccluded vertical FOV. Practically, there exists a minimum requirement for the slope angle to accommodate N imagers and an upper limit to avoid self-occlusion gap and to ensure view continuity. Therefore, the slope angle is constrained by

$$\frac{r_c}{2} \le \cos\alpha \le \sqrt{1 - \frac{r_c}{2\sin(\gamma/2)}}, \tag{4}$$

where the left side of the inequality assumes that half of the self-occlusion gap in (3) is equal to the complementary angle of the mirror slope; the right side of the inequality assumes that the N spheres enclosing each of the imagers are tangent to each other. For instance, given a six-sided pyramid, an imager-pyramid size ratio of 0.2 requires a slope angle of at least 26.6 degrees, which corresponds to a maximal, nonoccluded vertical FOV of 101.6 degrees and a self-occlusion gap of 25.2 degrees, and the same ratio requires a maximal slope angle of 84.26 degrees, which corresponds to zero degrees of nonoccluded vertical FOV.

Finally, the pyramid geometry should maintain a good shape factor and optimize sensor utilization. The effect of pyramid geometry on sensor usage will be further discussed in Section 4. Minimal pyramid geometry is defined as the one that provides the only but sufficient pyramid segments for capturing the continuous, nonoccluded reflective scene. The cap radius and shape factor of the minimal pyramid are given by

$$\begin{cases} r_a = r_d = \sin^2\alpha + \frac{r_c\cos\alpha}{2} \\ s_a = s_d = \sin\alpha\cos\alpha - \frac{r_c\sin\alpha}{2}. \end{cases} \tag{5}$$

Both the cap radius and shape factor of the minimal pyramid geometry are independent of the number of mirror faces in a pyramid. A small shape factor indicates a flat design and should be avoided. For a size ratio of 0.15, angles between 25 and 60 degrees will yield a pyramid with a shape factor better than 0.35.

4 Optical Constraints for Optimal Sensor Utilization

To understand how to select appropriate optical parameters of the imager clusters for optimal sensor utilization, in this section, we first determine the visual field reflected by a face (Section 4.1) and its mapping onto an image sensor (Section 4.2), and then analyze the conditions for optimizing image aspect ratio (Section 4.3), selection the imager FOV (Section 4.4), optimizing sensor efficiency (Section 4.5), and considering image uniformity (Section 4.6).

4.1 Reflective Visual Field

The reflective visual field is characterized by angles between the virtual optical axis of an imager and the principal ray of a scene point. Shown in Fig. 3a, the line connecting a point $P(x, y, z)$ on the mirror face $B_1B_2A_2A_1$ with the point O uniquely defines the principal ray of a scene point Q and the angle, θ_P, subtended by point P with the optical axis, OO_{11}, is given by

$$\cos\theta_P = \frac{x\cos\theta_T + z\sin\theta_T}{\sqrt{x^2 + y^2 + z^2}}. \tag{6}$$

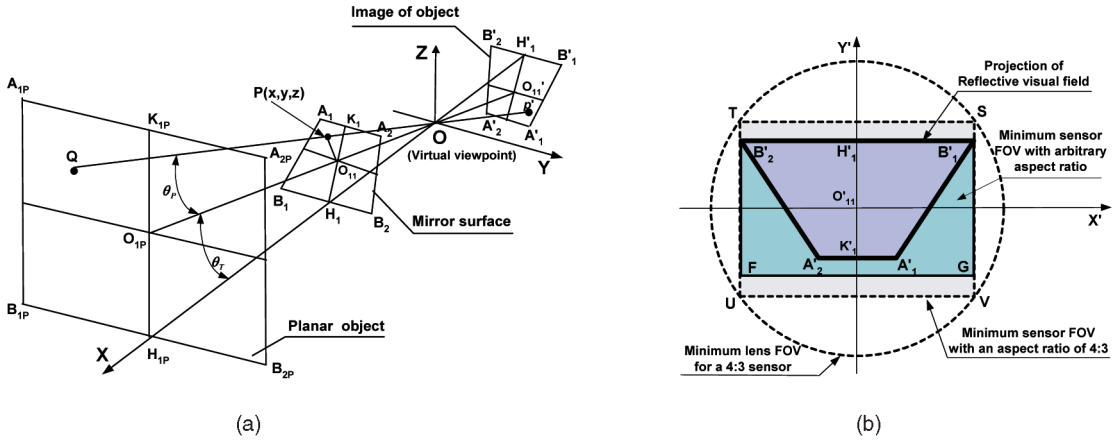

Fig. 3. Mapping reflective visual field to an image sensor: (a) Illustration of the reflective visual field formed by a mirror face. (b) Projection of the visual field and the size of sensor area.

The angles, θ_{B1}, θ_{A1}, θ_{H1}, and θ_{K1}, for the boundary points B_1, A_1, H_1, and K_1, respectively, are necessary to fully characterize the reflective visual fields. They are given by:

$$\begin{cases} \cos\theta_{B1} = \cos\theta_T \cos(\gamma/2) \\ \cos\theta_{A1} = \frac{\cos(\beta-\theta_T)\cos(\gamma/2)}{\sqrt{1-\sin^2\beta\sin^2(\gamma/2)}} \\ \theta_{H1} = \theta_T \\ \theta_{K1} = \beta - \theta_T, \end{cases} \tag{7}$$

where $\beta = \text{atan}(s_a/r_a)$ is the wedge angle of the pyramid (Fig. 1b).

4.2 Mapping the Reflective Visual Field to Image Sensor

To map the reflective visual field onto an image sensor, we assume that the imager lens is free from aberrations and the pinhole model applies. Practically, images must be rectified using the intrinsic parameters of the associated imagers obtained from a calibration process [20]. We further assume that the intersection of the optical axis OO_{11} with the sensor plane, O'_{11} is mapped to the central pixel of the image sensor (i.e., $u_0 = 0$, and $v_0 = 0$) (Fig. 3a). Therefore, the mapping point Q' for a scene point Q from the central pixel is given by $|O'Q'| = f\tan\theta_P$ and the mappings of the boundary points (Fig. 3b) are given by:

$$\begin{cases} |O'_{11}B'_1| = |O'_{11}B'_2| = f\cdot\tan\theta_{B1} \\ |O'_{11}A'_1| = |O'_{11}A'_2| = f\cdot\tan\theta_{A1} \\ |O'_{11}H'_1| = f\cdot\tan\theta_{H1} \\ |O'_{11}K'_1| = f\cdot\tan\theta_{K1}. \end{cases} \tag{8}$$

Points on a rectangular scene plane are mapped into a trapezoidal shape on the sensor and the scene is foreshortened due to the tilt of imagers.

4.3 Optimizing Aspect Ratio

The minimum sensor area required for each imager is illustrated as the rectangular area $B'_1B'_2FG$ in Fig. 3b, and its aspect ratio is calculated as

$$a = \frac{\sqrt{|O'_{11}B'_1|^2 - |O'_{11}H'_1|^2}}{\max(|O'_{11}H'_1|, |O'_{11}K'_1|)} = \frac{\tan(\gamma/2)}{\max(\tan(\theta_T), \tan(\beta-\theta_T))\cos\theta_T}. \tag{9}$$

Equation (9) indicates that the slope angle only affects the aspect ratio when $\theta_T \le \beta/2$, and increasing the number of pyramid faces reduces the aspect ratio. Imager orientation plays a critical role in affecting the aspect ratio and the aspect ratio is maximized at $\theta_T = \theta_1/2$.

To maximize sensor utilization, it is desirable to optimize the aspect ratio such that it closely matches with that of an actual image sensor, which often has a ratio of 4:3 or 3:4. Given slope angle $\alpha = 40^\circ$ and $r_c = 0.15$, Fig. 4 shows how the aspect ratio varies with the tilt angle θ_T and the number of mirror faces N. The results show that N is equal to 6 or 7 at $\theta_T = \theta_1/2$, N is equal to 4 at $\theta_T \approx 7^\circ$, and N is equal to 5 at $\theta_T \approx 13^\circ$ yield the closest match to the aspect ratio of 4:3. With the assumption of $r_c = 0.15$ and $\theta_T = \theta_1/2$, further examination of (9) suggests slope angles in the range of 30 to 60 degrees and $N \ge 6$ yield the closest match to the aspect ratio of 4:3.

4.4 Determining Imager FOV

It is critical to select an appropriate combination of imager sensor and lens that provides adequate FOV to capture the reflective visual field and maximize the sensor usage. The sensor FOV required for an imager with an arbitrary aspect ratio, illustrated as the rectangular area $B'_1B'_2FG$ in Fig. 3b, needs to meet the following conditions:

$$\begin{cases} \frac{p}{f} \ge 2\sqrt{\tan^2(\theta_{B1}) - \tan^2(\theta_{H1})} \\ \frac{q}{f} \ge 2\max(\tan(\theta_{H1}), \tan(\theta_{K1})) \\ \frac{\sqrt{p^2+q^2}}{f} \ge 2\tan(\theta_{B1}). \end{cases} \tag{10}$$

Assuming a sensor with an aspect ratio of 4:3, the minimal sensor FOV, illustrated as the rectangular area $STUV$ centered on O'_{11} in Fig. 3b, is usually larger than that depicted in (10). When the

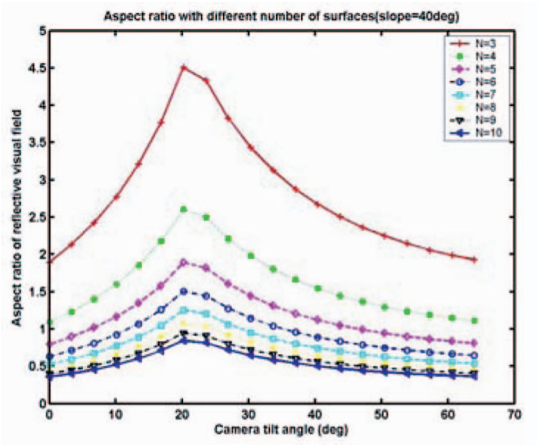

Fig. 4. Matching the aspect ratio of the reflective visual field with that of the sensor.

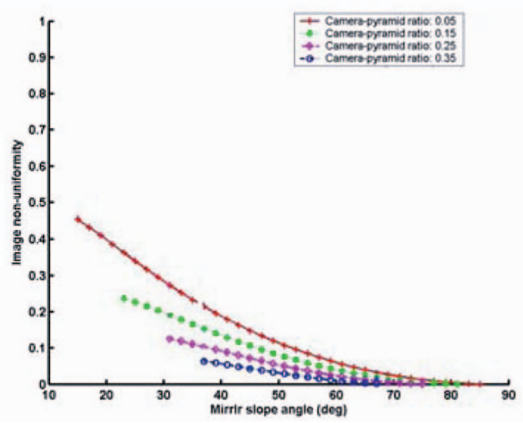

Fig. 5. At the optimal tilt condition, image nonuniformity decreases monotonically with increasing pyramid slope angle.

aspect ratio in (9) is greater than 1, the image sensor is positioned such that its long axis is parallel to the pyramid base, thus $q = \frac{3}{4}p$ is assumed; when the aspect ratio is less than 1, the image sensor is positioned such that its long axis is along the vertical visual field and $q = \frac{4}{3}p$ is assumed. Therefore, the minimal sensor FOV is uniquely characterized by $\frac{p}{f}|_{\min}$, the minimal ratio of horizontal sensor dimension to the focal length, and is given as

$$\frac{p}{f}\Big|_{\min} = \begin{cases} \max\left(\frac{2\tan(\gamma/2)}{\cos\theta_T}, \frac{8}{3}\max(\tan\theta_T, \tan(\beta-\theta_T)), \right. \\ \qquad \left. \frac{8\sqrt{1-\cos^2\theta_T\cos^2(\gamma/2)}}{5\cos\theta_T\cos(\gamma/2)}\right) & \text{a} \geq 1 \\ \max\left(\frac{2\tan(\gamma/2)}{\cos\theta_T}, \frac{3}{2}\max(\tan\theta_T, \tan(\beta-\theta_T)), \right. \\ \qquad \left. \frac{10\sqrt{1-\cos^2\theta_T\cos^2(\gamma/2)}}{3\cos\theta_T\cos(\gamma/2)}\right) & \text{a} < 1. \end{cases} \tag{11}$$

The horizontal FOV of the imager is calculated as $2\tan^{-1}(\frac{p}{f}|_{\min}/2)$ and the vertical FOV is calculated using the sensor's aspect ratio. The minimal FOV requirement in (11) is minimized at $\theta_T = \theta_1/2$.

4.5 Optimizing Sensor Efficiency

The utilization efficiency of the sensor, e, is defined as the ratio of the area covered by the nonoccluded reflective visual field to that of the image sensor. The maximum sensor efficiency, corresponding to the minimum sensor FOV in (11), is given as

$$\begin{aligned} e &= \frac{Area(\text{Reflective Visual Field})}{Area(\text{Minimum Sensor FOV})} \\ &= \begin{cases} \frac{3\tan(\gamma/2)\sin\beta(\cos(\beta-\theta_T)+\cos\beta\cos\theta_T)}{4\frac{p}{f}\big|_{\min}\cos^2\theta_T\cos^2(\beta-\theta_T)} & \text{a} < 1 \\ \frac{4\tan(\gamma/2)\sin\beta(\cos(\beta-\theta_T)+\cos\beta\cos\theta_T)}{3\frac{p}{f}\big|_{\min}\cos^2\theta_T\cos^2(\beta-\theta_T)} & \text{a} \geq 1. \end{cases} \end{aligned} \tag{12}$$

It is maximized when the tilt angle is selected such that the virtual axis of an imager bisects the achievable vertical FOV of a single pyramid. Thus, the optimal tilt angle of an imager is given by

$$\theta_T\big|_{opt} = \frac{\theta_1}{2} = \frac{90 - \alpha - \tan^{-1}(r_c/(2\sin\alpha))}{2}. \tag{13}$$

Given the condition in (13), the sensor efficiency can be further optimized by selecting an optimal combination of the pyramid slope angle and the number of mirror faces. For instance, N is equal to 5 for a slope angle of 29 degrees, N is equal to 6 for 41 degrees, and N is equal to 7 for 47 degrees to maximize sensor efficiency. Combining the considerations of vertical FOV and sensor efficiency, the optimal number of mirror faces is 6, and the optimal slope angle is about 40 degrees. This combination yields a sensor efficiency of 80 percent for an imager-pyramid size ratio of 5 percent, and 70 percent for a ratio of 25 percent.

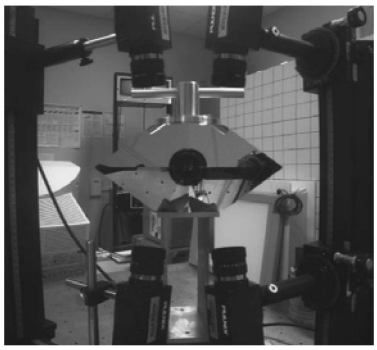

Fig. 6. The implementation of a six-sided DMP camera prototype.

4.6 Image Resolution and Uniformity

The effective number of pixels per imager for panoramic capture is given by $S \cdot T \cdot e$ and the overall pixel resolution of the entire panorama is $2N \cdot S \cdot T \cdot e$. The nonuniformity of the panorama, measured by the percentage of pixel differences between the bottom and top edges of the trapezoidal projection (Fig. 3b), is given by

$$\begin{aligned} U &= \frac{\sqrt{\tan^2\theta_{B1} - \tan^2\theta_{H1}} - \sqrt{\tan^2\theta_{A1} - \tan^2\theta_{K1}}}{\sqrt{\tan^2\theta_{B1} - \tan^2\theta_{H1}} + \sqrt{\tan^2\theta_{A1} - \tan^2\theta_{K1}}} \\ &= \frac{\sin\beta\sin\theta_T}{2\cos\beta\cos\theta_T + \sin\beta\sin\theta_T}. \end{aligned} \tag{14}$$

The image nonuniformity, independent of the number of mirror faces, decreases monotonically with increasing slope angles. While the optimal tilt angle in (13) maximizes the sensor usage, the image nonuniformity increases monotonically as the tilt angle increases. Given optimal tilt angles in (13), Fig. 5 illustrates how the nonuniformity is affected by pyramid geometry, which provides a guideline when a trade-off has to be made to balance sensor efficiency and image uniformity.

5 Prototype Implementation and Experimental Results

Using the constraints and relationships derived in Sections 3 and 4, we designed a panoramic camera with a right-hexagonal truncated DMP. The pyramid has a base radius of 115 mm and a slope angle of 40 degrees. The imagers selected are Pulnix cameras with 2/3″, 640×480 black/white CCD sensors. The imager-pyramid size ratio is about 0.2. The optimal cap radius of the pyramid is 56.3 mm, and the shape factor is 0.43. The imagers are tilted by 20.58 degrees relative to the pyramid base, yielding optimal sensor utilization. The aspect ratio of the reflective visual field is 1.64. The minimal FOV requirement for the imagers are 63.35 degrees and 47.49 degrees in the horizontal and vertical directions, respectively. The maximum focal length is 7.13 mm, which yields a panoramic camera with a sensor efficiency of 72 percent and image nonuniformity of 27 percent. A 6.5 mm lens was selected. This sensor-lens combination effectively provides a FOV of 68.2 degrees and 53.8 degrees for the horizontal and vertical directions, respectively, and yields a panoramic camera with an overall $360^\circ(H) * 82.4^\circ(V)$ nonoccluded FOV, a total of 2.176 Million pixels, sensor efficiency of 60 percent, and image nonuniformity of 27 percent. Each of the mirror faces effectively covers an FOV of 60 degrees horizontally and 41.2 degrees vertically.

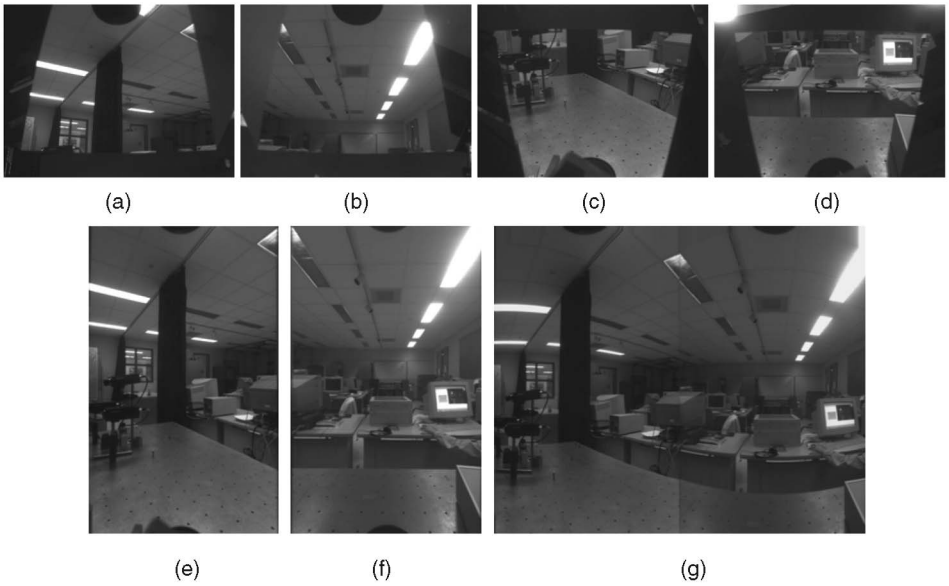

Fig. 7. Experimental results: (a), (b), (c), and (d) Original raw images. (e) and (f) The mosaics of images acquired by a pair of vertical imagers after postprocessing of distortions. (g) The cylindrical mosaic of the images (e) and (f).

Placing the imager clusters at the designated positions and attitudes with respect to the mirror pyramids is critical to the overall image quality and has proven to be an implementation challenge. Improper placement leads to visible seams or overlaps in resulting panoramas. Detail alignment and calibration procedures were discussed in [6]. Fig. 6 shows a final alignment of four imagers. Figs. 7a, 7b, 7c, and 7d show four images acquired by four adjacent imagers, two horizontally adjacent in the upper layer, the other two horizontally adjacent in the lower layer, and they are vertically adjacent. The inherent keystone distortion is caused by a tilt angle between the optical axis and pyramid base. The images of the reflective visual fields are compressed in their upper halves and enlarged in their lower halves. Each imager is calibrated to estimate its intrinsic and extrinsic parameters [20]. Along with radial distortion correction, a back-projection of a distorted image onto a virtual plane at an angle of $-\theta'_T$ degrees is applied to correct the keystone distortion, where θ'_T is the calibrated imager orientation. Then each vertical pair of dewarped images is concatenated to form a vertical mosaic with doubled FOV (Figs. 7e and 7f). The vertical mosaics are projected onto a cylinder centered at the common viewpoint to form the seamless mosaic. The resulting mosaic of the two vertical mosaic in Figs. 7e and 7f is shown in Fig. 7g.

6 Conclusion and Future Work

Several systems have been reported using reflections off planar mirror pyramids (MP) or prisms to achieve high resolution, wide-FOV, single or multiviewpoints, high-resolution, and real-time imaging. Using a DMP-based camera as an example, in this paper, we have investigated how the geometry of a mirror pyramid, and the selection and placement of imager clusters can be optimized to maximize the overall panoramic FOV, sensor utilization efficiency, and image uniformity. Based on the optimal design analysis, we have described the implementation of a DMP-based camera and included example images acquired. In the future work, we plan to extend the current four-imager implementation to a complete prototype with 12 calibrated imagers.

References

[1] S. Baker and S.K. Nayar, "A Theory of Single-Viewpoint Catadioptric Image Formation," *Int'l J. Computer Vision,* vol. 35, no. 2, pp. 1-22, 1999.

[2] R. Benosman and S.B. Kang, *Panoramic Vision: Sensors, Theory, and Applications.* Springer-Verlag, 2001.

[3] J.S. Chahl and M.V. Srinivasan, "Reflective Surfaces for Panoramic Imaging," *Applied Optics,* vol. 36, no. 31, pp. 8275-85, 1997.

[4] C. Gao, H. Hua, and N. Ahuja, "Method and Apparatus for a High-Resolution and Real-Time Panoramic Camera," US Patent 6,809,887 B1, 2004.

[5] R.A. Hicks and R. Bajcsy, "Catadioptric Sensors that Approximate Wide-Angle Perspective Projections," *Proc. IEEE Workshop Omnidirectional Vision,* pp. 97-103, 2000.

[6] H. Hua and N. Ahuja, "A High-Resolution Panoramic Camera," *Proc. Int'l Conf. Computer Vision and Pattern Recognition,* pp. 960-967, 2001.

[7] H. Ishiguro, M. Yamamoto, and S. Tsuji, "Omni-Directional Stereo," *IEEE Trans. Pattern Analysis and Machine Intelligence,* vol. 14, no. 2, pp. 257-262, Feb. 1992.

[8] T. Kawanishi and K. Yamazawa, "Generation of High Resolution Stereo Panoramic Images by Omnidirectional Imaging Sensor Using Hexagonal Pyramidal Mirrors," *Proc. 14th Int'l Conf. Pattern Recognition,* pp. 485-489, 1998.

[9] A. Krishnan and N. Ahuja, "Panoramic Image Acquisition," *Proc. Int'l Conf. Computer Vision and Pattern Recognition,* pp. 379-384, 1996.

[10] A. Majumder, W. Brent Seals, M. Gopi, and H. Fuchs, "Immersive Teleconferencing: A New Algorithm to Generate Seamless Panoramic Video Imagery," *Proc. ACM Multimedia,* pp. 169-178, 1999.

[11] V. Nalwa, "A True Omnidirectional Viewer," technical report, Bell Laboratories, Feb. 1996.

[12] V. Nalwa, "Compact High-Resolution Panoramic Viewing System," US Patent 6,195,204B1, 2001.

[13] V. Nalwa, "Panoramic Viewing System with a Composite Field of View," US Patent 6,700,711, 2004.

[14] S.K. Nayar, "Catadioptric Omnidirectional Camera," *Proc. Int'l Conf. Computer Vision and Pattern Recognition,* pp. 482-488, 1997.

[15] http://www.ptgrey.com/products/spherical.html, 2006.

[16] S. Peleg, "Panoramic Mosaics by Manifold Projection," *Proc. Int'l Conf. Computer Vision and Pattern Recognition,* pp. 338-343, 1997.

[17] K.H. Tan, H. Hua, and N. Ahuja, "Multiview Panoramic Cameras Using Mirror Pyramid," *IEEE Trans. Pattern Analysis and Machine Intelligence,* vol. 26, no. 7, pp. 941-946, July 2004.

[18] Y. Xiong and K. Turkowski, "Creating Image-Based VR Using a Self-Calibrating Fisheye Lens," *Proc. Int'l Conf. Computer Vision and Pattern Recognition,* pp. 237-243, 1997.

[19] K. Yamazawa, Y. Yagi, and M. Yachida, "Omnidirectional Imaging with Hyperboloidal Projection," *Proc. Int'l Conf. Intelligent Robots and Systems,* pp. 1029-1034, 1993.

[20] Z. Zhang, "A Flexible New Technique for Camera Calibration," Technical Report MSR-TR-98-71, Microsoft Research, 1998.

[21] Z. Zhu, K.D. Rajasekar, E.M. Riseman, and A.R. Hanson, "Panoramic Virtual Stereo Vision of Cooperative Mobile Robots for Localizing 3D Moving Objects," *Proc. IEEE Workshop Omnidirectional Vision,* pp. 29-36, 2000.